

AMXFP4: TAMING ACTIVATION OUTLIERS WITH ASYMMETRIC MICROSCALING FLOATING-POINT FOR 4-BIT LLM INFERENCE

Janghwan Lee¹ Jiwoong Park¹ Jinseok Kim² Yongjik Kim² Jungju Oh² Jinwook Oh² Jungwook Choi¹

ABSTRACT

Scaling Large Language Models (LLMs) with extended context lengths has increased the need for efficient low-bit quantization to manage their substantial computational demands. However, reducing precision to 4 bits frequently degrades performance due to activation outliers. To address this, we propose Asymmetric Microscaling 4-bit Floating-Point (AMXFP4) for efficient LLM inference. This novel data format leverages asymmetric shared scales to mitigate outliers while naturally capturing the asymmetry introduced by group-wise quantization. Unlike conventional 4-bit quantization methods that rely on data rotation and costly calibration, AMXFP4 uses asymmetric shared scales for direct 4-bit casting, achieving near-ideal quantization accuracy across various LLM tasks, including multi-turn conversations, long-context reasoning, and visual question answering. Our AMXFP4 format significantly outperforms MXFP4 and other leading quantization techniques, enabling robust, calibration-free 4-bit inference. Our code is available at [aiha-lab/MX-QLLM.git](https://github.com/aiha-lab/MX-QLLM).

1 INTRODUCTION

Multi-modal Large Language Models (LLMs) are increasingly utilized for advanced natural language processing tasks, supporting applications such as chatbots, long-document question-answering, and visual graph interpretation (Touvron et al., 2023; Bai et al., 2023; Liu et al., 2023a). LLMs have been scaled significantly in parameter size to enhance their capabilities and trained to handle extended context lengths (Chung et al., 2022; Chowdhery et al., 2022; AI@Meta, 2024). For instance, LLaMA3 now encompasses 405 billion parameters and supports context lengths of up to 128K tokens. As shown in Fig. 1(a), this scaling leads to computational demands in the peta-FLOP (floating-point operation) range just for the prefill phase, where the model processes the user’s context in preparation for inference. This surge in computational demand underscores the need for innovation in computational platforms.

Leading computing platforms have prioritized bit-precision scaling to meet LLM’s high computational demands (Andersch et al., 2022; Nvidia, 2024; AzureAI, 2024). As demonstrated in (Horowitz, 2014), reducing operand bit-widths enhances area and energy efficiency in arithmetic logic operations, enabling higher computation density in accelerators. For instance, NVIDIA’s Tensor Cores doubled its computation speed (FLOPS) by reducing multiply-

¹Department of Electronic Engineering, Hanyang University, Seoul, Republic of Korea ²Rebellions Inc., Republic of Korea. Correspondence to: Jungwook Choi <choij@hanyang.ac.kr>.

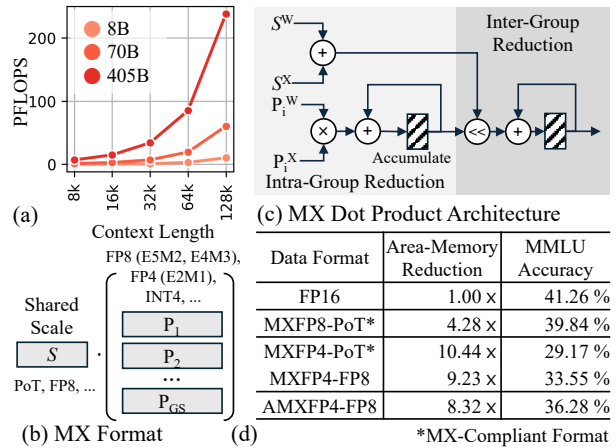


Figure 1. (a) FLOPS across context length and model sizes. (b) MX format and (c) dot-product unit. (d) Comparison of the area-memory product and LLaMA2-7B MMLU scores against FP16.

accumulate (MAC) precision from FP16 to FP8 (Andersch et al., 2022). A recent advance in precision-scaling is the microscaling (MX) format introduced by the Open Compute Project (Rouhani et al., 2023a). As shown in Fig. 1(b), the MX format groups elements in low precision with a shared scale compensating for their limited dynamic range. This group-wise data representation decouples intra-group dot products from group-wise scaling, enabling efficient MAC implementations with minimal overhead from inter-group scale adjustments (Fig. 1(c)). Our MX-compatible MAC unit implementation, based on the micro-architecture in

(Darvish Rouhani et al., 2023), shows that 8-bit and 4-bit MX formats reduce area-memory costs by over $4\times$ and $8\times$, respectively (Fig. 1(d)). This aligns with MXFP4’s early adoption in recent deep learning accelerators, offering a $2\times$ speedup over 8-bit computation (Nvidia, 2024; AzureAI, 2024). However, MXFP4’s robustness for LLM inference remains underexplored: our evaluation on LLaMA2 reveals significant degradation on MMLU benchmarks compared to MXFP8, consistent with findings in (Rouhani et al., 2023b). This underscores the need for data format innovation for robust 4-bit inference.

From an algorithmic perspective, active research has been conducted on activation and weight quantization for efficient LLM inference. Performance degradation in LLMs due to quantizing both weights and activations is often attributed to the difficulty of handling activation outliers (Dettmers et al., 2022; Xiao et al., 2022). Recent studies transform activation data with outliers into forms more suitable for quantization through rotation, achieving state-of-the-art LLM accuracy with 4-bit integer (INT4) weight and activation (Ashkboos et al., 2024; Liu et al., 2024c). However, these methods rely on model pre-processing to calibrate the rotation matrix, presenting three main drawbacks (Lee et al., 2023; Lin et al., 2023). First, the calibration process is costly, requiring carefully prepared datasets that may involve data refinement and raise security/privacy concerns. Second, the calibration process is time-consuming as it involves weight parameter adjustment or additional training. Third, models can overfit to the calibration dataset, limiting general deployment. In addition to these drawbacks, the rotation methods exclude quantization for the Softmax output, leaving a significant portion of computation in FP16 for long-context inference (cf. Fig. 2(a) and (b)). Thus, developing a generalizable quantization method that enables direct-casting of all matrix multiplication and avoids calibration overhead is essential.

In this work, we introduce AMXFP4, an innovative microscaling floating-point format for robust 4-bit LLM inference that effectively addresses activation outliers through micro-scaled asymmetric data representation. Our format builds on an in-depth analysis of MX format’s ability to handle activation outliers. Notably, grouping activation tensors into small micro-scaled units mitigates outlier effects, similar to rotation methods but without costly calibration. This grouping, however, increases data asymmetry, necessitating an asymmetric numerical representation. Through extensive evaluation of various data formats, we develop asymmetric microscaled FP4 with an FP8 shared scale (AMXFP4-FP8), achieving quantization error rates close to those of ideal Lloyd-Max quantization. The AMXFP4-based MAC unit implementation benefits from amortized shared-scale adjustments, adding only 10% to the hardware cost over the MXFP4 design while achieving over $8\times$ efficiency (Fig. 1(d)). To validate AMXFP4’s broad

applicability, we conduct comprehensive evaluations across diverse LLM benchmarks, including multi-turn conversation, long-context inference, and visual question-answering (VQA) tasks on decoder-only LLMs, vision-language models, and an encoder-decoder model. Our results demonstrate that AMXFP4 enables calibration-free direct-cast 4-bit inference, significantly outperforming both MXFP4 and the state-of-the-art 4-bit quantization methods.

Our contributions can be summarized as follows:

- We examine the MXFP4 format, finding that microscaling effectively reduces activation outliers without costly calibration but introduces asymmetry, necessitating asymmetric numerical representation.
- We propose AMXFP4-FP8, a novel format that combines FP4 elements with shared asymmetric FP8 scales, enabling low-overhead computation and significantly suppressing quantization error.
- We evaluate AMXFP4 across diverse applications, including multi-turn conversation, long-context inference, and VQA, across multiple model types, demonstrating consistently superior performance to MXFP4 and the top-notch rotation-based quantization methods.

2 BACKGROUND AND RELATED WORK

2.1 Bit-Precision Scaling for Accelerators

Reduced-precision data formats are vital for enhancing scalability and computational efficiency in deep learning accelerators, conserving area and energy in direct proportion to bit-width reduction (Horowitz, 2014). This scaling enables higher floating-point operations per second (FLOPS) with lower power usage, thereby increasing accelerator throughput. For instance, NVIDIA’s Tensor Cores have progressed from FP16 in Volta (Nvidia, 2017) to FP8 in Hopper (Andersch et al., 2022) and FP4 in Blackwell (Nvidia, 2024), boosting computational speeds from 112 tera to 20 peta FLOPS. Similar advancements by other computing platform companies in scaling precision from 16-bit to 4-bit are crucial for managing the growing complexity of LLMs (AMD, 2024; AzureAI, 2024).

Reduced-precision computation takes advantage of neural networks’ resilience to small numerical errors, though aggressive scaling often results in accuracy loss. To address this, various algorithmic enhancements have been developed. Early methods introduced formats like BFloat16 (Burgess et al., 2019) and DLFloat (Agrawal et al., 2019) to optimize the exponent and mantissa trade-off. More recent research has advanced 8-bit (Wang et al., 2018; Sun et al., 2019) and 4-bit (Sun et al., 2020) formats, although FP4 has shown noticeable accuracy degradation. To enhance

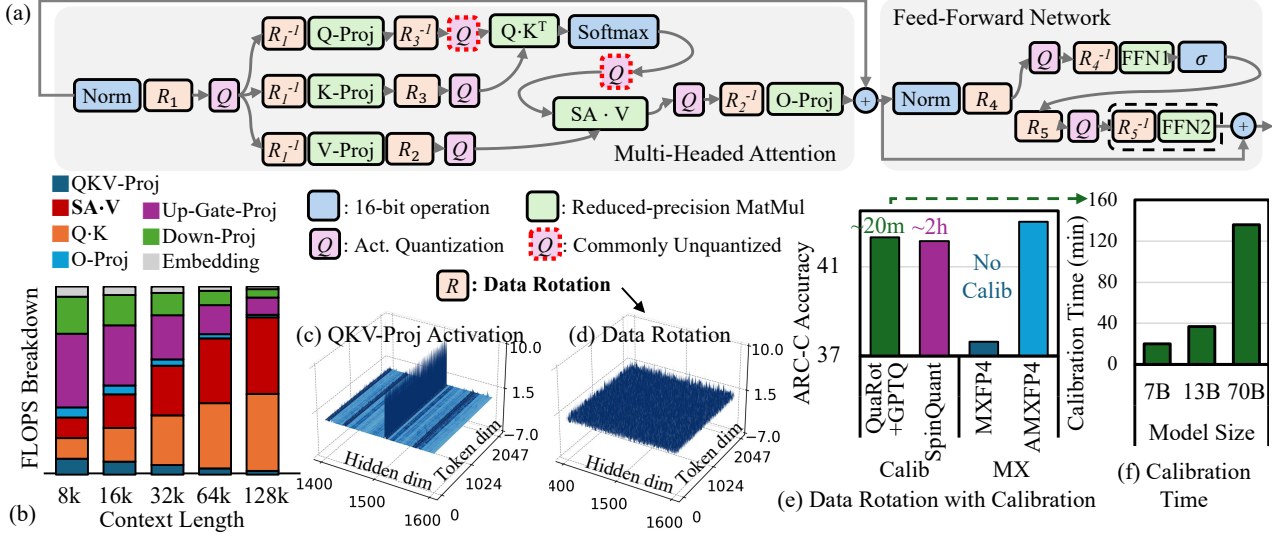


Figure 2. (a) Illustration of where reduced-precision matrix multiplication and data transformation are applied within a Transformer decoder layer. QuaRot and SpinQuant do not quantize the Query and Softmax outputs (red dotted box). (b) FLOPS breakdown of LLaMA3-8B in the prefill stage based on context length. (c-d) Distribution of LLM activation outliers before and after data rotation application (LLaMA2-7B layer 1 QKV-proj input activation). (e) Accuracy comparison between calibration-based methods and MX (LLaMA2-7B). (f) Calibration time (measured in single A100 GPU) requirements according to model size.

low-precision LLM inference, the microscaling (MX) format (Rouhani et al., 2023a; Darvish Rouhani et al., 2023; Rouhani et al., 2023b) has been developed from Block Floating Point (BFP) (Drumond et al., 2018; Darvish Rouhani et al., 2020) by incorporating a shared scale across a block of reduced-precision elements, thus mitigating quantization error due to limited dynamic range. While the original BFP format allows flexibility in design parameters—exponent (E) and mantissa (M) for the element (P_i) and the shared scale (S), and the group size (GS), the MX format prescribes specific *MX-compliant* configurations: MXFP8-PoT ($P_i: E5M2/E4M3$, $S: E8$ (= power-of-two), $GS: 32$) and MXFP4-PoT ($P_i: E2M1$, $S: E8$, $GS: 32$), as shown in Fig. 1(b) and (d).

To demonstrate the hardware efficiency of MX format, we implemented the MX-compatible MAC unit using the microarchitecture (cf. Fig. 1(c)) in (Darvish Rouhani et al., 2023) on Synopsys Design Compiler with a 4nm node and a target frequency of 1.1GHz. As shown in Fig. 1(d), the 8-bit and 4-bit MX formats reduce area-memory costs by over 4× and 8×, respectively. This efficiency stems from the group-wise data representation, which separates intra-group dot products from group-wise scaling, minimizing overhead from inter-group scale adjustments.

However, MXFP4’s robustness for LLM inference remains uncertain, with significant performance degradation in 4-bit inference due to activation quantization (Rouhani et al., 2023b). This aligns with our evaluation of LLaMA2

(Fig. 1(d)), which shows substantial degradation on MMLU benchmarks compared to MXFP8. Moreover, MXFP4 lacks validation on practical tasks such as multi-turn chatbot interactions, raising concerns about its real-world applicability. While MXFP4 models generate coherent answers, they often yield unhelpful responses, consistent with findings that quantization can impair conversational quality (Lee et al., 2024) (e.g., Fig. 6). These results underscore the need for new data formats to enable robust 4-bit inference.

2.2 Quantizing LLM’s Activation and Weight

Recent research highlights the difficulty quantifying LLM activations due to outliers extending the activation dynamic range, leading to increased quantization error (Xiao et al., 2022; Ashkboos et al., 2024). Prior studies propose rescaling weights and activations to reshape their distributions for better quantization compatibility while preserving mathematical equivalence (Xiao et al., 2022; Shao et al., 2024; Lee et al., 2023). However, such methods often experience performance degradation in 4-bit inference (Lin et al., 2024). Data rotation strategies, including QuaRot (Ashkboos et al., 2024) and SpinQuant (Liu et al., 2024c), use orthogonal matrices to redistribute concentrated channel information (represented as R in Fig. 2(a)). QuaRot applies a randomized Hadamard matrix, while SpinQuant uses learned rotation matrices. DuQuant further enhances this approach by combining per-channel permutation and rotation, achieving state-of-the-art performance in 4-bit inference (Lin et al.,

2024). As illustrated in Fig. 2(d), the rotation matrix effectively disperses activation outliers, making the distribution more suitable for low-bit quantization.

However, These rotation-based methods exclude quantization for the Softmax output, leaving matrix multiplications in the self-attention calculation to be computed in FP16 (indicated by dotted quantization in Fig. 2(a)). This mixed-precision setup adds considerable computational overhead, especially in long-context inference, as self-attention computation scales quadratically with context length in the prefill phase. As shown in Fig. 2(b), the FLOPS for self-attention (SA) times value (V) grow rapidly with increasing context length. Therefore, the partial quantization of the rotation methods diminishes overall computational efficiency, leading to significant overhead in long-context processing.

Moreover, these rotation-based techniques depend heavily on additional calibration processes, such as GPTQ or training rotation matrices, to boost performance, introducing several key challenges. Calibration requires carefully curated datasets, often demanding extensive data refinement, which raises privacy and security concerns (Lee et al., 2023; Lin et al., 2023). The calibration process is also resource-intensive, involving weight adjustments or additional training, making it increasingly time-consuming with model size. As illustrated in Fig. 2(e), calibration can increase model accuracy (LLaMA2 evaluated on ARC-Challenge (Clark et al., 2018), but this improvement comes at the expense of added calibration time, which further increases with model size (Fig. 2(f)). This prolongs development cycles and complicates deployment for larger models using rotation-based quantization. Additionally, calibration risks overfitting, as models may become too tailored to the calibration dataset, limiting adaptability across broader applications.

These combined challenges highlight the need for a generalizable quantization approach that minimizes calibration dependence and applies uniformly across computations. Although MXFP4, a previously explored reduced-precision format, applies to all matrix multiplication without calibration, it compromises model accuracy. This work analyzes MXFP4’s limitations and proposes AMXFP4, a superior 4-bit format that enables direct-casting with improved model accuracy.

3 MICROSCALING FOR TAMING OUTLIERS

In this section, we systematically analyze activation outliers across various LLMs using representative statistical measures—kurtosis and mean—to understand the effects of microscaling (i.e., reducing a quantization group to 32 elements). Kurtosis, the fourth standardized moment, is commonly used to assess the prevalence of outliers (Liu et al., 2024c; Li et al., 2024), while the mean reflects asym-

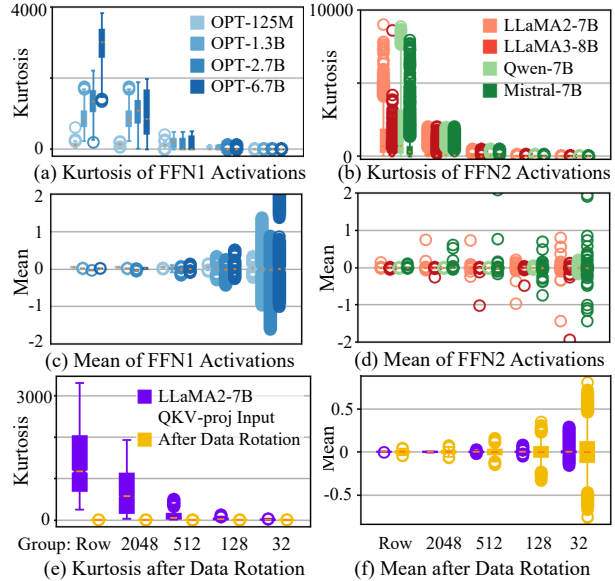


Figure 3. LLM data characteristics based on (a-d) types of model, layer and (e-f) data rotation across group sizes.

metry within each group. We use box plots of kurtosis and mean to examine the value distribution within groups, which are subject to quantization using a shared scale.

3.1 Analysis of LLM’s Activation Outliers

Fig. 3(a) and (b) present the kurtosis box plots for the OPT (Zhang et al., 2022) and LLaMA-like models (LLaMA, Qwen, Mistral (Touvron et al., 2023; AI@Meta, 2024; Bai et al., 2023; Jiang et al., 2023)). In cases of row-wise grouping (typically $GS \gg 1024$), the OPT models exhibit high kurtosis in FFN1 activations, indicating many outliers that challenge quantization. Additionally, outlier prevalence increases with model size, aligning with previous findings that larger models are more affected by quantization (Dettmers et al., 2022). Conversely, LLaMA-like models use the Gated Linear Unit (GLU) activation function, involving extra matrix multiplication; thus, data passing through FFN1 undergoes element-wise multiplication before FFN2, further amplifying outliers—a phenomenon observed in recent studies (Yang et al., 2024; Fishman et al., 2024). Notably, outlier dominance is reduced as group size decreases in both model types. At $GS = 32$, kurtosis nearly disappears, suggesting the activation dynamic range within groups becomes more suitable for quantization. This observation helps explain the preliminary success of MXFP8 in direct-casting for selected LLMs (Rouhani et al., 2023b), but it does not explain the disappointing performance of MXFP4.

To assess the trade-offs in the MX format’s handling of outliers, we examine the box plots of group means, which reflect distribution asymmetry. Fig. 3(c) and (d) show the

mean values for FFN1 and FFN2 input activations as group size decreases from an entire row to 32. Notably, with large group sizes, group means center around zero, but as group size decreases, the means scatter significantly. This scattering indicates that the symmetric data representation typically used in the MX format is suboptimal for microscaled activation quantization. In other words, *microscaling addresses activation outliers at the cost of data symmetry*. Thus, simply reducing group size (as in the MX format) may not adequately minimize quantization error; instead, an asymmetric data representation becomes essential.

3.2 Data Rotation vs. Microscaling

We then examine how data rotation reduces outliers alongside microscaling and assess its effectiveness as group size decreases. Fig. 3(e) shows the kurtosis before and after applying data rotation using a random Hadamard transform across decreasing group sizes. When the group size spans an entire row, activation rotation substantially lowers kurtosis, demonstrating its efficacy in 4-bit activation quantization. However, as group size decreases, the original activation’s kurtosis also drops, reaching levels comparable to those achieved with rotation. Thus, the benefit of data rotation in outlier reduction diminishes with smaller group sizes.

On the other hand, Fig. 3(f) shows the group means of the activation before and after applying data rotation. As with the original activation, the group means scatter more as group sizes decrease, but this scattering is even more pronounced with rotated activations. This indicates that rotation introduces an additional asymmetry in group distributions, which complicates quantization with MXFP4’s symmetric representation (cf. Table 4). In other words, data rotation and microscaling lack synergy, as both focus on outlier suppression without addressing asymmetry. Given data rotation’s dependence on calibration, developing a new microscaling data format that can handle group distribution asymmetry becomes increasingly compelling.

3.3 Multi-modal LLM’s Activation Outlier

To further understand activation outliers under microscaling in multi-modal LLMs, we examine the popular vision-language model LLaVA (Liu et al., 2023a). LLaVA combines a visual encoder and a language model backbone: an image is processed by a vision transformer-based encoder (ViT, (Dosovitskiy et al., 2021)) to generate vision tokens, which are then input to the language model along with language tokens from the user prompt.

As shown in Fig. 4(a), both vision and language tokens exhibit outliers within the same hidden dimension of the activation, though their distributions differ. Language tokens typically concentrate around larger magnitudes, while only some vision tokens reach high magnitudes, a trend observed

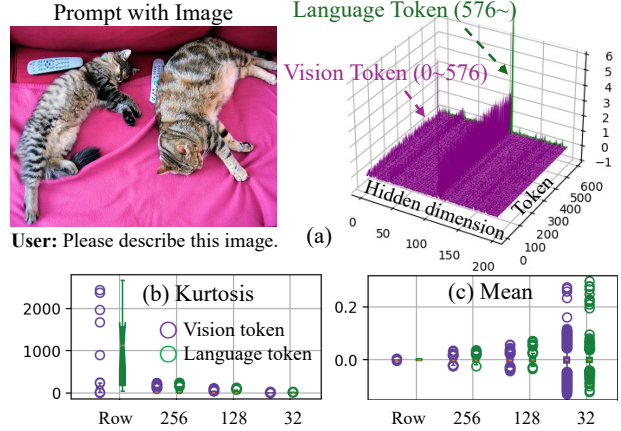


Figure 4. Characteristic of VLM activation outliers across group sizes (LLaVA-v1.6-Vicuna-7B Layer 1 QKV-Proj).

consistently across layers. In Fig. 4(c), these differences result in varying kurtosis distributions for row-wise group quantization: language tokens have clustered outliers, while vision tokens show a sparser outlier distribution. However, this distinction fades as group size decreases, illustrating the effectiveness of microscaling in suppressing outliers. Similar to LLMs, LLaVA’s group means scatter as group size decreases, indicating increased asymmetry in exchange for outlier suppression. This suggests microscaling could better handle diverse outlier patterns from vision and language tokens if designed to support asymmetric data representation.

4 ASYMMETRIC MICROSCALING FORMAT

The findings from Sec. 3 motivate the development of a new microscaling format that inherently supports asymmetric data representation. In this section, we explore the design space of the microscaling data format (P_i and S) alongside considerations for asymmetric quantization schemes to enable efficient MAC unit implementation.

4.1 Asymmetric Quantization

We consider two popular asymmetric quantization schemes: asymmetric INT (AsymINT) and asymmetric FP (AsymFP).

Asymmetric INT Quantization (AsymINT). In INT quantization, asymmetry is applied through a zero-point, shifting the data range from zero-centered to span between the minimum and maximum values, represented uniformly in reduced-precision integers (Dettmers et al., 2022). Multiplying two AsymINT numbers incurs computational overhead due to cross-terms associated with the zero-point (see Appendix B.3 for details).

Asymmetric FP Quantization (AsymFP). In FP quanti-

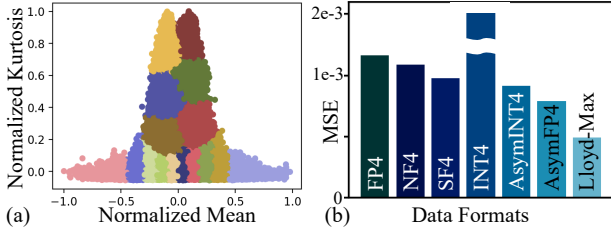


Figure 5. Cluster-wise Lloyd-Max quantization and quantization error across data formats (LLaMA2-7B layer 5 QKV-Proj input activation).

zation, asymmetry is applied to the scale due to FP’s inherently zero-centered representation (Zhang et al., 2024b). An exponent-bit-shifted mantissa represents a value, then multiplied by either a positive or negative shared scale based on the sign. Formally, we define AsymFP as follows:

$$x_q = \begin{cases} (-1)^s \cdot 2^{E+eb} \cdot M \cdot (2^{seb_p} \cdot \hat{M}_p) & \text{if } s = 0, \\ (-1)^s \cdot 2^{E+eb} \cdot M \cdot (2^{seb_n} \cdot \hat{M}_n) & \text{if } s = 1, \end{cases} \quad (1)$$

where s , E , eb , and M represent an element’s sign, exponent, exponent bias, and mantissa, respectively. The terms $2^{seb_p} \cdot \hat{M}_p$ and $2^{seb_n} \cdot \hat{M}_n$ denote the positive and negative scales shared within a quantization group.

4.2 Selecting Element-Wise Data Format

First, we explore the design space of the data format for each element P_i . To understand the benefits of asymmetric data format, we compare the mean-square error (MSE) on example activation data (sampled from LLaMA2-7B’s QKV-Proj at layer 5) with other symmetric data format (FP4, NF4 (Dettmers et al., 2023), SF4 (Dotzel et al., 2024)). Fig. 5(a) shows the characteristics of this activation in terms of group means (x-axis) and kurtosis (y-axis). As a reference, we cluster the groups based on similarity in mean and kurtosis, then conduct Lloyd-Max algorithm (Lloyd, 1982) for close-to-ideal quantized number representation (100 iterations; the number of clusters is set as 16, as no further MSE reduction observed from more clusters).

Fig. 5(b) presents the MSE of various element-wise data formats. Compared to Lloyd-Max quantization (used as a reference), all symmetric data formats show a significant MSE increase, with INT4 experiencing the most notable degradation. In contrast, AsymINT4 and AsymFP4 achieve lower MSE, with AsymFP showing MSE closest to Lloyd-Max (a consistent trend across models and layers). This finding supports the selection of AsymFP4 as the element-wise format, further validated empirically in Table 2.

4.3 Selecting Shared-Scale

With AsymFP4 selected as the preferred element-wise data representation, we further examine options for shared positive and negative scales (variations in the exponent and mantissa in Eq. 1) for efficient MAC unit implementation.

PoT: When $\hat{M}_p = \hat{M}_n = 1$, the dynamic range for positive and negative values can be adjusted via exponent modification. For AMX, an additional shift operation is required in the intra-level reduction in Fig. 1(d) to account for positive and negative scales. We found that the 5-bit PoT avoids significant clamping errors for quantizing large magnitude values (see Appendix A.2 for more details).

FP8: While a 5-bit PoT scale prevents clamping errors, its limited resolution still causes accuracy degradation. To address this, we propose using FP8 scales, which significantly reduce memory requirements and minimize resource overhead for multiplication due to a shorter mantissa than FP16. With a 5-bit exponent, $E5M2$ effectively mitigates accuracy loss from a limited dynamic range (see Table 16 for ablation studies). FP8 scales require additional multiplication of the mantissas for positive and negative scales depending on the operand’s sign; however, this incurs minimal resource overhead due to the small mantissa size, and once calculated, the overhead is shared within a group. Our evaluation shows that AMXFP4-FP8 incurs only a 10% overhead compared to MXFP4-FP8 (Fig. 1(d)).

5 EXPERIMENTS

5.1 Impact of Microscaling and Data Rotation

Sec. 3.2 demonstrates that data rotation effectively addresses activation outliers in configurations with large group sizes but shows limited compatibility with microscaling. We examine the impact of data rotation on Wikitext-2 (Merity et al., 2016) perplexity across group sizes from an entire row to 32 in Table 1. For the data rotation, we apply a randomized Hadamard transform matrix (following (Ashkboos et al., 2024)) and quantize the input operands for all matrix multiplications within the decoder layer. When the group size encompasses an entire row, MXFP8-PoT maintains performance close to the baseline, with MXFP6-PoT experiencing only minimal performance loss. For LLaMA2-13B, MXFP4-FP8 undergoes a notable increase in perplexity, while AMXFP4-FP8 reduces perplexity to approximately 34. Importantly, data rotation substantially lowers perplexity to around 11 without the need for asymmetric representation, highlighting its effectiveness in handling outliers with larger group sizes. However, as the group size decreases, data rotation significantly increases perplexity by 3.6 in LLaMA2-7B with MXFP4-FP8, whereas AMXFP4-FP8 achieves a reduction of 0.3 in the same model. This result aligns with our finding that outlier handling becomes less

AMXFP4: Taming Activation Outliers with Asymmetric Microscaling Floating-Point for 4-bit LLM Inference

Group Size	Data Rotation	Data Format	LLaMA			Mistral 7B
			7B	13B	8B	
FP16 Baseline			5.5	4.9	6.1	5.3
Row	-	MXFP8-PoT	5.6	5.0	6.3	5.3
		MXFP6-PoT	5.8	5.1	6.7	5.4
		MXFP4-FP8	475.6	99.3	85.1	80.6
		AMXFP4-FP8	44.8	33.8	40.3	26.0
	✓	MXFP8-PoT	5.5	4.9	6.3	5.3
		MXFP6-PoT	5.9	5.1	6.8	5.4
		MXFP4-FP8	11.9	10.8	13.3	6.9
		AMXFP4-FP8	12.0	11.5	12.1	6.8
256	-	MXFP6-PoT	5.7	5.1	6.7	5.5
		MXFP4-FP8	7.8	7.0	11.2	6.7
		AMXFP4-FP8	7.1	6.2	9.2	6.2
	✓	MXFP6-PoT	5.9	5.1	6.8	5.4
		MXFP4-FP8	14.0	7.7	10.8	6.6
		AMXFP4-FP8	10.8	6.8	10.0	6.4
32	-	MXFP4-FP8	6.5	5.7	8.4	5.8
		AMXFP4-FP8	6.2	5.5	7.7	5.7
	✓	MXFP4-FP8	10.1	6.9	9.5	6.3
		AMXFP4-FP8	8.4	6.4	9.2	6.2

Table 1. Wikitext-2 perplexity results by group size with and without data rotation applied across microscaling formats (lower is better).

Data Rotation	Data Format	GS=Row	GS=128	GS=32
FP16 Baseline		5.47		
-	INT4	NaN	10.06	6.73
	AsymINT4	2951.92	6.99	6.10
	FP4	350.26	7.06	6.21
	AsymFP4	29.78	6.56	6.00
✓	INT4	41.19	9.86	7.66
	AsymINT4	17.08	7.62	6.52
	FP4	26.10	19.19	10.74
	AsymFP4	24.01	13.23	7.94

Table 2. Wikitext-2 perplexity results by group size with and without data rotation (lower is better), evaluated on LLaMA2-7B for both INT and FP data formats.

effective as the group size decreases.

We extend our experiments to the INT in Table 2 to determine whether the adverse effects of data rotation stem from the non-uniform data representation characteristic of FP. In this experiment, we use an FP16 shared scale to eliminate the impact of shared scaling across the two different formats. When the group size spans an entire row, INT4 experiences a significant increase in perplexity, which asymmetric representation reduces to approximately 2951. Notably, data rotation reduces perplexity to around 41, achieving the lowest perplexity when combined with asymmetric representation. However, at a group size of 32, data rotation tends to increase perplexity in both INT and FP formats. While AsymINT4 achieves lower perplexity than either INT4 or FP4, AsymFP4 yields the lowest perplexity overall. This suggests that our data format selection for microscaling is appropriate and indicates that data rotation does not enhance microscaling performance, regardless of the data format.

5.2 Comparison with Calibration-Based Methods

We investigate the influence of the calibration dataset on outlier handling techniques and examine the calibration overhead of these methods. Additionally, we compare our approach with state-of-the-art (SOTA) techniques for weight-activation quantization. In this section, we omit quantization for activations in cases where previous studies do not apply it (e.g. Softmax output), in order to evaluate whether our proposed MX format can directly replace existing outlier handling techniques. Detailed experimental settings are provided in Appendix B.2.

Robustness to Calibration Set Distributions. We investigate the sensitivity of QuaRot and SpinQuant to different calibration set distributions, as shown in Table 3. We measure perplexity (PubMed (of the U.S. National Library of Medicine, 2023) and Enron Emails (Klimt & Yang, 2004)) and accuracy (PIQA (Bisk et al., 2019) and WinoGrande (Sakaguchi et al., 2019)) under conditions where the calibration and evaluation datasets are the same and where they differ. Details on the composition of the calibration dataset are provided in the Appendix B.2. QuaRot and SpinQuant significantly improve performance over random Hadamard rotation but show a clear pattern of achieving better results on data observed during calibration. There is an exception that SpinQuant achieves high performance on both PIQA and WinoGrande when PIQA data is used for calibration, though a 2-3% performance difference arises solely from varying calibration datasets, indicating that calibration-based methods are highly dataset-sensitive. MXFP4-PoT is unaffected by the calibration set but exhibits severe performance degradation, whereas the proposed AMXFP4-FP8 significantly enhances performance, surpassing traditional calibration-based methods.

Calibration Overhead and Performance Variation. Table 4 displays the effects of varying calibration settings (dataset, sequence length, and number of samples) on Wikitext-2 perplexity, ARC-Challenge (Clark et al., 2018) and WinoGrande accuracy for QuaRot and SpinQuant. When using QuaRot alone, CSQA accuracy drops by 10%. When combined QuaRot with GPTQ, results depend on calibration settings; using only 32 calibration samples leads to a 2.4% reduction in WinoGrande accuracy compared to using 128 samples. SpinQuant, which trains a rotation matrix, achieves higher accuracy than QuaRot alone but increases calibration time by approximately 6× and exhibits greater sensitivity to the calibration set. When calibrated with the PTB (Marcus et al., 1993) dataset instead of Wikitext-2, perplexity on Wikitext-2 rises by around 0.9. The proposed AMXFP4 shows minimal performance degradation compared to the baseline and remains unaffected by calibration settings.

Comparison with Other 4-bit Inference Methods. Ta-

AMXFP4: Taming Activation Outliers with Asymmetric Microscaling Floating-Point for 4-bit LLM Inference

Model	Evaluation Set	Random Rotation	QuaRot+GPTQ		SpinQuant		MXFP4-PoT	MXFP4-FP8	AMXFP4-FP8
Calibration Dataset		-	PubMed	Enron	PubMed	Enron	-	-	-
LLaMA2 -7B	PubMed ↓	7.65	5.37	5.45	5.71	5.86	6.00	5.36	5.28
	EnRon ↓	7.94	6.33	6.21	6.75	6.32	6.94	6.24	6.14
LLaMA3 -8B	PubMed ↓	9.41	7.40	7.60	7.45	7.70	7.77	6.96	6.80
	EnRon ↓	12.89	10.65	10.20	10.65	9.98	10.85	9.64	9.36
Calibration Dataset		-	PIQA	Wino	PIQA	Wino	-	-	-
LLaMA2 -7B	PIQA ↑	72.03	77.37	76.17	76.44	73.07	76.71	77.48	77.80
	Wino ↑	60.14	65.27	65.90	66.38	64.01	66.93	67.88	67.48

Table 3. Impact of overfitting: Calibration on different data distribution on LLaMA models.

Rotation	Calibset- SeqLen-Samples	Calib. Time (A100)	PPL↓			Accuracy↑		
			Wiki	ARC-C	WG	Wiki	ARC-C	WG
16-bit Baseline			5.47	46.33	69.30			
QuaRot	-	-	8.38	36.26	60.06			
QuaRot+ GPTQ	Wiki-2048-128	~20 min	6.08	41.64	66.22			
	Wiki-1024-128		6.06	42.32	65.59			
	Wiki-2048-64		6.11	41.64	65.51			
	Wiki-2048-32		6.11	41.55	63.85			
	PTB-2048-128		6.16	42.15	65.43			
	PTB-1024-128		6.12	41.72	66.54			
SpinQuant	Wiki-2048-100	~2 hours	6.25	38.65	64.72			
	Wiki-1024-100		6.32	40.87	63.77			
	PTB-2048-100		7.11	38.74	60.30			
	PTB-1024-100		7.14	37.71	63.54			
AMXFP4-FP8 (direct-cast, no calibration)			5.93	42.83	67.32			

Table 4. Calibration overhead on LLaMA2-7B.

Method	Format	Direct-cast?	1-7B	1-13B	2-7B	2-13B
16-bit Baseline			5.68	5.09	5.47	4.88
SmoothQuant			25.25	40.05	83.12	35.88
OmniQuant			11.26	10.87	14.26	12.30
AffineQuant			10.28	10.32	12.69	11.45
QLLM	INT	no	9.65	8.41	11.75	9.09
Atom			8.15	7.43	8.40	6.96
DuQuant			6.40	5.65	6.28	5.42
AMXFP4-FP8			MX	yes	6.17	5.46

Table 5. Comparison with SOTA quantization methods for 4-bit inference on Wikitext-2 inference with LLaMA models. Perplexities of INT techniques are adapted from (Lin et al., 2024)

Table 5 compares 4-bit inference results across various weight-activation quantization techniques, including AMXFP4. The SOTA method, DuQuant (Lin et al., 2024), achieves a significant reduction in perplexity, outperforming other techniques. Meanwhile, AMXFP4 attains performance comparable to SOTA methods without requiring calibration. This suggests that AMXFP4 offers an effective solution for sustaining high performance in quantized models while reducing calibration dependence—an important advantage for practical deployment scenarios that demand adaptability and minimal performance loss.

More Aggressive Quantization. To explore the potential future of the proposed microscaling format, we compare AMXFP with QuaRot and MXFP at settings lower than 4-bit.

Method	Format	Direct-cast?	LLaMA2-7B	LLaMA2-13B
16-bit Baseline			5.47	4.88
QuaRot-RTN			1032.30	1105.95
QuaRot-GPTQ	INT	no	38.47	37.42
MXFP3-PoT	MX	yes	NaN	39.79
AMXFP3-FP8			8.40	6.53

Table 6. Wikitext-2 perplexity results on 3-bit inference.

Table 6 shows the inference results for the LLaMA2 model at 3-bit. In 3-bit inference, QuaRot with GPTQ shows significant performance degradation. MXFP3-PoT also experiences a significant deterioration in perplexity. Conversely, AMXFP3-FP8 demonstrates a significant improvement in perplexity, indicating that our findings are effective at lower bit settings. This underscores the robustness of AMXFP in maintaining performance with reduced bit precision, potentially paving the way for more efficient computational models in resource-constrained environments.

5.3 Enhancing MX Performance

We experiment with AMXFP4-FP8 across various benchmarks, including chatbot, visual, and long-context tasks, to explore the practical advantages of our proposed data format in real-world applications compared to MXFP4-PoT. Experimental details, including quantization settings and benchmarks, are provided in Appendix B.1.

Multi-Turn Chatbot Tasks. Quantization adversely affects the conversational capabilities of chatbots (Lee et al., 2024); therefore, we conduct an MT-Bench evaluation (Zheng et al., 2023) on LLaMA2-Chat-7B (Touvron et al., 2023) to determine whether AMXFP4-FP8 significantly improves conversational abilities compared to MXFP4-PoT. MT-Bench assigns scores ranging from 1 to 10, given by GPT-4 (OpenAI, 2023), to responses generated from an initial question and a subsequent follow-up question across 80 multi-turn conversations. Fig. 6 presents the normalized scores of MXFP4-PoT, MXFP4-FP8, and AMXFP4-FP8, with the 16-bit baseline score set to 1. While MXFP4-PoT inference shows severe performance degradation across all categories, AMXFP4-FP8 demonstrates recovery of conversational abilities close to the baseline. Fig. 10 provides detailed ex-

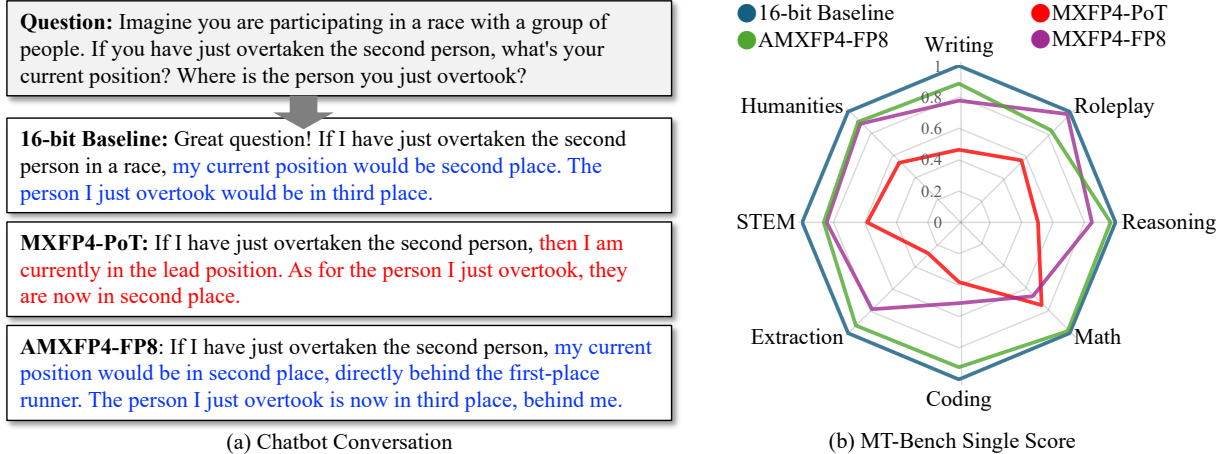


Figure 6. MT-Bench example and normalized single score (LLaMA2-Chat-7B). Absolute accuracies are in Table 14 in Appendix.

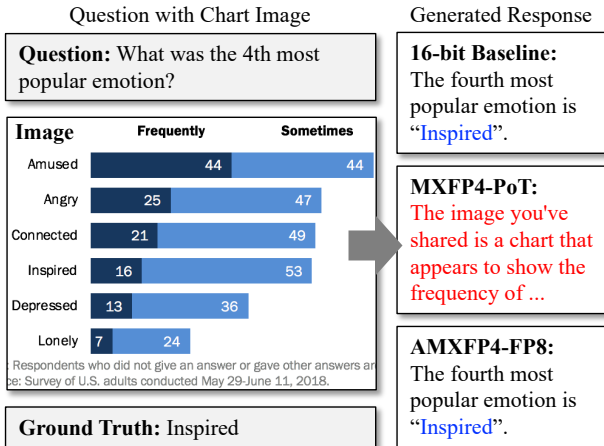


Figure 7. Comparison between responses from MXFP4-PoT and AMXFP4-FP8 in ChartQA example.

amples, showing that while MXFP4 generates unhelpful sentences, AMXFP4 produces responses that are genuinely helpful.

Visual Tasks. We extend our experiments to multi-modal benchmarks with LLaVA1.6-7B (Liu et al., 2023a). Table 7 presents results on four multi-modal benchmarks (Zhang et al., 2024a) where both images and questions are provided. MXFP4-PoT shows a score degradation of over 10, whereas

Data Format	VQA-T	DocVQA	OCRBench	ChartQA
16-bit Baseline	64.84	74.46	52.40	54.72
MXFP4-PoT	50.05	52.85	33.70	36.76
MXFP4-FP8	57.88	64.26	43.40	46.20
AMXFP4-PoT	53.19	56.55	37.20	39.80
AMXFP4-FP8	59.13	66.98	43.90	49.48

Table 7. LLaVA1.6-7B inference results on multi-modal visual question-answering benchmarks.

Data Format	OPT		LLaMA			Mistral
	6.7B	13B	2-7B	2-13B	3-8B	7B
16-bit Baseline	10.86	10.13	5.47	4.88	6.14	5.25
MXFP4-PoT	25.51	12.88	7.83	6.98	11.17	6.34
MXFP4-FP8	13.71	12.09	6.49	5.69	8.31	5.88
AMXFP4-PoT	25.00	12.65	7.46	6.60	10.05	6.19
AMXFP4-FP8	13.06	11.90	6.22	5.47	7.72	5.71

Table 8. Wikitext-2 inference for MXFP4 and AMXFP4.

MXFP4-FP8 improves overall performance through an enhanced shared scale. AMXFP4-FP8 further increases the score by around 3.3 on benchmarks such as ChartQA (Masry et al., 2022), demonstrating the significant benefits of asymmetric data representation in VLM.

Long-Context Tasks. We conduct the LongBench-E (Bai et al., 2024) evaluation to assess the effectiveness of AMXFP4 in long-context scenarios. Through LongBench-E, we measure performance across 13 benchmarks and categorize average scores by context length. As shown in Fig. 8(a), MXFP4-PoT suffers significant performance degradation when addressing questions with lengthy contexts. While MXFP4-FP8 generally improves scores, AMXFP4-FP8 demonstrates further performance gains, even with context lengths exceeding 8k. As illustrated in Fig. 8(b-c), when questions require referencing multiple lengthy passages, MXFP4-PoT tends to generate incorrect answers, whereas AMXFP4-FP8 provides answers identical to the baseline, underscoring the practical benefits of this performance improvement in real-world applications.

Language Modeling Tasks. Table 8 presents Wikitext-2 perplexity results for six LLMs across MXFP4 and AMXFP4 with PoT and FP8 shared scale. While MXFP4-PoT introduces significant perplexity degradation across all models, employing MXFP4-FP8 with an enhanced shared scale substantially reduces perplexity in each case. No-

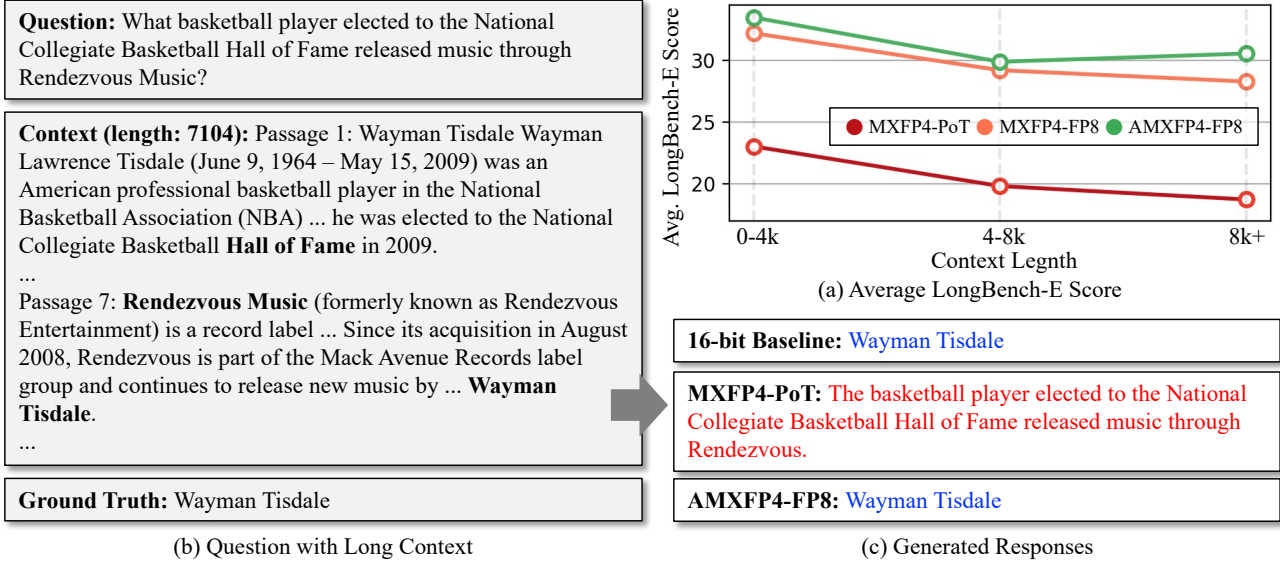


Figure 8. LongBench-E results on LLaMA2-Chat-7B. Detailed scores are in Table 15.

Data Format	OPT		LLaMA			Mistral 7B	Avg.
	6.7B	13B	2-7B	2-13B	3-8B		
16-bit Baseline	58.9	59.2	64.9	67.3	69.2	70.0	64.9
MXFP4-PoT	47.3	55.7	59.4	62.1	58.6	64.0	57.9
MXFP4-FP8	54.4	57.4	61.6	65.1	62.0	66.4	61.1
AMXFP4-PoT	48.1	56.2	59.2	62.6	59.3	64.6	58.3
AMXFP4-FP8	55.9	56.3	62.0	64.9	62.2	67.4	61.4

Table 9. Zero-shot CSQA accuracy for MXFP4 and AMXFP4.

tably, AMXFP4-FP8, through asymmetric data representation, achieves a 0.59 perplexity reduction in LLaMA3-8B compared to MXFP4-FP8 and limits perplexity degradation to only about 0.46 in models like Mistral-7B.

Knowledge Evaluation Benchmarks. We implement successive enhancements to the MXFP4 format and evaluate their impact on the Common-Sense Question Answering (CSQA) (Talmor et al., 2019) and MMLU (Hendrycks et al., 2020) benchmarks. As shown in Table 9, AMXFP4-FP8 significantly improves performance compared to MXFP4-PoT. Notably, as presented in Table 10, these performance gains are even more pronounced in the MMLU benchmark. While MXFP4-FP8 substantially improves upon the performance of MXFP4-PoT, AMXFP4-FP8 further enhances the MMLU score by approximately 3% in all models.

Encoder-Decoder Language Model. Table 11 displays the ROUGE (Lin, 2004) scores for BART-Large’s (Lewis et al., 2019) summarization task on the CNN/DailyMail dataset (See et al., 2017) across different MX format options. AMXFP4-FP8 exhibits only a 0.7-point drop in ROUGE-L score compared to the baseline, demonstrating that the proposed data format also enables effective 4-bit inference in encoder-decoder models.

LLaMA	Data Format	Hums	STEM	Social	Other	Avg.
2-7B	16-bit Baseline	38.7	34.5	46.2	47.2	41.3
	MXFP4-PoT	28.3	28.0	30.2	30.6	29.2
	MXFP4-FP8	31.7	30.3	36.4	36.9	33.5
	AMXFP4-PoT	28.6	28.1	30.3	31.4	29.5
2-13B	AMXFP4-FP8	34.4	32.1	39.6	40.1	36.3
	16-bit Baseline	47.1	40.9	58.5	57.5	50.5
	MXFP4-PoT	36.4	31.3	41.9	42.8	37.9
	MXFP4-FP8	40.3	36.0	49.2	47.1	42.8
3-8B	AMXFP4-PoT	38.2	31.3	44.2	42.9	39.0
	AMXFP4-FP8	42.6	37.1	51.6	49.9	45.0
	16-bit Baseline	54.8	53.3	73.0	71.0	62.0
	MXFP4-PoT	38.4	37.7	50.3	48.8	43.1
3-8B	MXFP4-FP8	44.8	42.4	57.9	55.3	49.5
	AMXFP4-PoT	40.8	39.9	52.8	51.7	45.6
	AMXFP4-FP8	47.2	44.0	62.7	60.5	52.8

Table 10. MMLU inference results for MXFP4 and AMXFP4.

Data Format	ROUGE-1 ↑	ROUGE-2 ↑	ROUGE-L ↑
16-bit Baseline	45.09	21.60	31.43
MXFP4-PoT	42.47	19.10	29.18
MXFP4-FP8	43.73	20.50	30.43
AMXFP4-PoT	43.06	19.59	29.66
AMXFP4-FP8	44.13	20.79	30.72

Table 11. CNN/DailyMail summarization task on BART-Large.

6 CONCLUSION

To meet the computational demands of large language models (LLMs) with extended contexts, we introduce Asymmetric Microscaling 4-bit Floating-Point (AMXFP4), which uses asymmetric shared scales to handle outliers and quantization asymmetry. Unlike traditional methods requiring costly calibration, AMXFP4 provides direct 4-bit inference with high accuracy, outperforming MXFP4 and other techniques for efficient, calibration-free inference.

REFERENCES

- Agrawal, A., Mueller, S. M., Fleischer, B. M., Sun, X., Wang, N., Choi, J., and Gopalakrishnan, K. Dfloat: A 16-b floating point format designed for deep learning training and inference. In *2019 IEEE 26th Symposium on Computer Arithmetic (ARITH)*, pp. 92–95. IEEE, 2019.
- AI@Meta. Llama 3 model card. 2024. URL https://github.com/meta-llama/llama3/blob/main/MODEL_CARD.md.
- AMD. Amd instinct™ mi325x accelerators. <https://www.amd.com/content/dam/amd/en/documents/instinct-tech-docs/product-briefs/instinct-mi325x-datasheet.pdf>, 2024.
- Andersch, M., Palmer, G., Krashinsky, R., Stam, N., Mehta, V., Brito, G., and Ramaswamy, S. Nvidia hopper architecture in-depth. <https://developer.nvidia.com/blog/nvidia-hopper-architecture-in-depth/>, 2022.
- Ashkboos, S., Mohtashami, A., Croci, M. L., Li, B., Jaggi, M., Alistarh, D., Hoefler, T., and Hensman, J. Quarot: Outlier-free 4-bit inference in rotated llms. *arXiv preprint arXiv:2404.00456*, 2024.
- AzureAI. Azure maia for the era of ai: From silicon to software to systems. <https://azure.microsoft.com/en-us/blog/azure-maia-for-the-era-of-ai-from-silicon-to-software-to-systems/>, 2024.
- Bai, J., Bai, S., Chu, Y., Cui, Z., Dang, K., Deng, X., Fan, Y., Ge, W., Han, Y., Huang, F., et al. Qwen technical report. *arXiv preprint arXiv:2309.16609*, 2023.
- Bai, Y., Lv, X., Zhang, J., Lyu, H., Tang, J., Huang, Z., Du, Z., Liu, X., Zeng, A., Hou, L., Dong, Y., Tang, J., and Li, J. LongBench: A bilingual, multitask benchmark for long context understanding. In Ku, L.-W., Martins, A., and Srikumar, V. (eds.), *Proceedings of the 62nd Annual Meeting of the Association for Computational Linguistics (Volume 1: Long Papers)*, pp. 3119–3137, Bangkok, Thailand, August 2024. Association for Computational Linguistics. doi: 10.18653/v1/2024.acl-long.172. URL <https://aclanthology.org/2024.acl-long.172>.
- Bisk, Y., Zellers, R., Bras, R. L., Gao, J., and Choi, Y. Piqa: Reasoning about physical commonsense in natural language, 2019.
- Bisk, Y., Zellers, R., Bras, R. L., Gao, J., and Choi, Y. Piqa: Reasoning about physical commonsense in natural language. In *Thirty-Fourth AAAI Conference on Artificial Intelligence*, 2020.
- Burgess, N., Milanovic, J., Stephens, N., Monachopoulos, K., and Mansell, D. Bfloat16 processing for neural networks. In *2019 IEEE 26th Symposium on Computer Arithmetic (ARITH)*, pp. 88–91. IEEE, 2019.
- Chiang, W.-L., Li, Z., Lin, Z., Sheng, Y., Wu, Z., Zhang, H., Zheng, L., Zhuang, S., Zhuang, Y., Gonzalez, J. E., Stoica, I., and Xing, E. P. Vicuna: An open-source chatbot impressing gpt-4 with 90%* chatgpt quality, March 2023. URL <https://lmsys.org/blog/2023-03-30-vicuna/>.
- Chowdhery, A., Narang, S., Devlin, J., Bosma, M., Mishra, G., Roberts, A., Barham, P., Chung, H. W., Sutton, C., Gehrmann, S., et al. Palm: Scaling language modeling with pathways. *arXiv preprint arXiv:2204.02311*, 2022.
- Chung, H. W., Hou, L., Longpre, S., Zoph, B., Tay, Y., Fedus, W., Li, E., Wang, X., Dehghani, M., Brahma, S., et al. Scaling instruction-finetuned language models. *arXiv preprint arXiv:2210.11416*, 2022.
- Clark, P., Cowhey, I., Etzioni, O., Khot, T., Sabharwal, A., Schoenick, C., and Tafjord, O. Think you have solved question answering? try arc, the ai2 reasoning challenge. *arXiv:1803.05457v1*, 2018.
- Darvish Rouhani, B., Lo, D., Zhao, R., Liu, M., Fowers, J., Ovtcharov, K., Vinogradsky, A., Massengill, S., Yang, L., Bittner, R., et al. Pushing the limits of narrow precision inferencing at cloud scale with microsoft floating point. *Advances in neural information processing systems*, 33: 10271–10281, 2020.
- Darvish Rouhani, B., Zhao, R., Elango, V., Shafipour, R., Hall, M., Mesmakhosroshahi, M., More, A., Melnick, L., Golub, M., Varatkar, G., et al. With shared microexperts, a little shifting goes a long way. In *Proceedings of the 50th Annual International Symposium on Computer Architecture*, pp. 1–13, 2023.
- Dasigi, P., Lo, K., Beltagy, I., Cohan, A., Smith, N. A., and Gardner, M. A dataset of information-seeking questions and answers anchored in research papers. 2021.
- Dettmers, T., Lewis, M., Belkada, Y., and Zettlemoyer, L. Llm.int8(): 8-bit matrix multiplication for transformers at scale. *arXiv preprint arXiv:2208.07339*, 2022.
- Dettmers, T., Pagnoni, A., Holtzman, A., and Zettlemoyer, L. QLoRA: Efficient finetuning of quantized LLMs. In *Thirty-seventh Conference on Neural Information Processing Systems*, 2023. URL <https://openreview.net/forum?id=OUIFPHEgJU>.
- Dosovitskiy, A., Beyer, L., Kolesnikov, A., Weissenborn, D., Zhai, X., Unterthiner, T., Dehghani, M., Minderer, M., Heigold, G., Gelly, S., Uszkoreit, J., and Houlsby,

- N. An image is worth 16x16 words: Transformers for image recognition at scale. In *International Conference on Learning Representations*, 2021. URL <https://openreview.net/forum?id=YicbFdNTTy>.
- Dotzel, J., Chen, Y., Kotb, B., Prasad, S., Wu, G., Li, S., Abdelfattah, M. S., and Zhang, Z. Learning from students: Applying t-distributions to explore accurate and efficient formats for llms. *International Conference on Machine Learning*, 2024.
- Drumond, M., Lin, T., Jaggi, M., and Falsafi, B. Training dnns with hybrid block floating point. *Advances in Neural Information Processing Systems*, 31, 2018.
- Fishman, M., Chmiel, B., Banner, R., and Soudry, D. Scaling fp8 training to trillion-token llms, 2024. URL <https://arxiv.org/abs/2409.12517>.
- Gao, L., Biderman, S., Black, S., Golding, L., Hoppe, T., Foster, C., Phang, J., He, H., Thite, A., Nabeshima, N., et al. The pile: An 800gb dataset of diverse text for language modeling. *arXiv preprint arXiv:2101.00027*, 2020.
- Gao, L., Tow, J., Biderman, S., Black, S., DiPofi, A., Foster, C., Golding, L., Hsu, J., McDonell, K., Muennighoff, N., Phang, J., Reynolds, L., Tang, E., Thite, A., Wang, B., Wang, K., and Zou, A. A framework for few-shot language model evaluation, September 2021. URL <https://doi.org/10.5281/zenodo.5371628>.
- Gliwa, B., Mochol, I., Biesek, M., and Wawer, A. SAM-Sum corpus: A human-annotated dialogue dataset for abstractive summarization. In Wang, L., Cheung, J. C. K., Carenini, G., and Liu, F. (eds.), *Proceedings of the 2nd Workshop on New Frontiers in Summarization*, pp. 70–79, Hong Kong, China, November 2019. Association for Computational Linguistics. doi: 10.18653/v1/D19-5409. URL <https://aclanthology.org/D19-5409>.
- Guo, D., Xu, C., Duan, N., Yin, J., and McAuley, J. Long-coder: A long-range pre-trained language model for code completion, 2023. URL <https://arxiv.org/abs/2306.14893>.
- Hendrycks, D., Burns, C., Basart, S., Zou, A., Mazeika, M., Song, D., and Steinhardt, J. Measuring massive multitask language understanding. *CoRR*, abs/2009.03300, 2020. URL <https://arxiv.org/abs/2009.03300>.
- Ho, X., Duong Nguyen, A.-K., Sugawara, S., and Aizawa, A. Constructing a multi-hop QA dataset for comprehensive evaluation of reasoning steps. In Scott, D., Bel, N., and Zong, C. (eds.), *Proceedings of the 28th International Conference on Computational Linguistics*, pp. 6609–6625, Barcelona, Spain (Online), December 2020. International Committee on Computational Linguistics. doi: 10.18653/v1/2020.coling-main.580. URL <https://aclanthology.org/2020.coling-main.580>.
- Horowitz, M. Energy table for 45nm process, 2014.
- Huang, L., Cao, S., Parulian, N., Ji, H., and Wang, L. Efficient attentions for long document summarization. In Toutanova, K., Rumshisky, A., Zettlemoyer, L., Hakkani-Tur, D., Beltagy, I., Bethard, S., Cotterell, R., Chakraborty, T., and Zhou, Y. (eds.), *Proceedings of the 2021 Conference of the North American Chapter of the Association for Computational Linguistics: Human Language Technologies*, pp. 1419–1436, Online, June 2021. Association for Computational Linguistics. doi: 10.18653/v1/2021.naacl-main.112. URL <https://aclanthology.org/2021.naacl-main.112>.
- Jiang, A. Q., Sablayrolles, A., Mensch, A., Bamford, C., Chaplot, D. S., Casas, D. d. l., Bressand, F., Lengyel, G., Lample, G., Saulnier, L., et al. Mistral 7b. *arXiv preprint arXiv:2310.06825*, 2023.
- Joshi, M., Choi, E., Weld, D., and Zettlemoyer, L. triviaqa: A Large Scale Distantly Supervised Challenge Dataset for Reading Comprehension. *arXiv e-prints*, art. arXiv:1705.03551, 2017.
- Klimt, B. and Yang, Y. The enron corpus: A new dataset for email classification research. 2004. URL <https://api.semanticscholar.org/CorpusID:13451873>.
- Lee, J., Kim, M., Baek, S., Hwang, S., Sung, W., and Choi, J. Enhancing computation efficiency in large language models through weight and activation quantization. In Bouamor, H., Pino, J., and Bali, K. (eds.), *Proceedings of the 2023 Conference on Empirical Methods in Natural Language Processing*, pp. 14726–14739, Singapore, December 2023. Association for Computational Linguistics. doi: 10.18653/v1/2023.emnlp-main.910. URL <https://aclanthology.org/2023.emnlp-main.910>.
- Lee, J., Park, S., Hong, S., Kim, M., Chang, D.-S., and Choi, J. Improving conversational abilities of quantized large language models via direct preference alignment. In Ku, L.-W., Martins, A., and Srikumar, V. (eds.), *Proceedings of the 62nd Annual Meeting of the Association for Computational Linguistics (Volume 1: Long Papers)*, pp. 11346–11364, Bangkok, Thailand, August 2024. Association for Computational Linguistics. doi: 10.18653/v1/2024.acl-long.612. URL <https://aclanthology.org/2024.acl-long.612>.

- Lewis, M., Liu, Y., Goyal, N., Ghazvininejad, M., Mohamed, A., Levy, O., Stoyanov, V., and Zettlemoyer, L. Bart: Denoising sequence-to-sequence pre-training for natural language generation, translation, and comprehension. *arXiv preprint arXiv:1910.13461*, 2019.
- Li, S., Ning, X., Wang, L., Liu, T., Shi, X., Yan, S., Dai, G., Yang, H., and Wang, Y. Evaluating quantized large language models, 2024. URL <https://arxiv.org/abs/2402.18158>.
- Li, X. and Roth, D. Learning question classifiers. In *COLING 2002: The 19th International Conference on Computational Linguistics*, 2002. URL <https://aclanthology.org/C02-1150>.
- Lin, C.-Y. ROUGE: A package for automatic evaluation of summaries. In *Text Summarization Branches Out*, pp. 74–81, Barcelona, Spain, July 2004. Association for Computational Linguistics. URL <https://aclanthology.org/W04-1013>.
- Lin, H., Xu, H., Wu, Y., Cui, J., Zhang, Y., Mou, L., Song, L., Sun, Z., and Wei, Y. Duquant: Distributing outliers via dual transformation makes stronger quantized llms, 2024. URL <https://arxiv.org/abs/2406.01721>.
- Lin, J., Tang, J., Tang, H., Yang, S., Dang, X., and Han, S. Awq: Activation-aware weight quantization for llm compression and acceleration. *arXiv*, 2023.
- Liu, H., Li, C., Wu, Q., and Lee, Y. J. Visual instruction tuning. In Oh, A., Naumann, T., Globerson, A., Saenko, K., Hardt, M., and Levine, S. (eds.), *Advances in Neural Information Processing Systems*, volume 36, pp. 34892–34916. Curran Associates, Inc., 2023a. URL https://proceedings.neurips.cc/paper_files/paper/2023/file/6dcf277ea32ce3288914faf369fe6de0-Paper-Conference.pdf.
- Liu, J., Gong, R., Wei, X., Dong, Z., Cai, J., and Zhuang, B. QLLM: Accurate and efficient low-bitwidth quantization for large language models. In *International Conference on Learning Representations (ICLR)*, 2024a.
- Liu, T., Xu, C., and McAuley, J. Repobench: Benchmarking repository-level code auto-completion systems, 2023b. URL <https://arxiv.org/abs/2306.03091>.
- Liu, Y., Li, Z., Huang, M., Yang, B., Yu, W., Li, C., Yin, X., lin Liu, C., Jin, L., and Bai, X. Ocrbench: On the hidden mystery of ocr in large multimodal models, 2024b. URL <https://arxiv.org/abs/2305.07895>.
- Liu, Z., Zhao, C., Fedorov, I., Soran, B., Choudhary, D., Krishnamoorthi, R., Chandra, V., Tian, Y., and Blankevoort, T. Spinqtant-llm quantization with learned rotations. *arXiv preprint arXiv:2405.16406*, 2024c.
- Lloyd, S. Least squares quantization in pcm. *IEEE Transactions on Information Theory*, 28(2):129–137, 1982. doi: 10.1109/TIT.1982.1056489.
- Ma, Y., Li, H., Zheng, X., Ling, F., Xiao, X., Wang, R., Wen, S., Chao, F., and Ji, R. Affinequant: Affine transformation quantization for large language models. In *The Twelfth International Conference on Learning Representations*, 2024. URL <https://openreview.net/forum?id=of2rhALq81>.
- Marcus, M. P., Santorini, B., and Marcinkiewicz, M. A. Building a large annotated corpus of English: The Penn Treebank. *Computational Linguistics*, 19(2):313–330, 1993. URL <https://aclanthology.org/J93-2004>.
- Masry, A., Long, D., Tan, J. Q., Joty, S., and Hoque, E. ChartQA: A benchmark for question answering about charts with visual and logical reasoning. In *Findings of the Association for Computational Linguistics: ACL 2022*, pp. 2263–2279, Dublin, Ireland, May 2022. Association for Computational Linguistics. doi: 10.18653/v1/2022.findings-acl.177. URL <https://aclanthology.org/2022.findings-acl.177>.
- Mathew, M., Karatzas, D., and Jawahar, C. V. Docvqa: A dataset for vqa on document images, 2021. URL <https://arxiv.org/abs/2007.00398>.
- Merity, S., Xiong, C., Bradbury, J., and Socher, R. Pointer sentinel mixture models, 2016.
- Nvidia. Nvidia tesla v100 gpu architecture. 2017. URL <https://images.nvidia.com/content/volta-architecture/pdf/volta-architecture-whitepaper.pdf>.
- Nvidia. Nvidia blackwell architecture technical brief. 2024. URL <https://resources.nvidia.com/en-us-blackwell-architecture>.
- of the U.S. National Library of Medicine, C. Pubmed. <https://huggingface.co/datasets/ncbi/pubmed>, 2023.
- OpenAI. Gpt-4 technical report. *arXiv preprint arXiv:2303.08774*, 2023.
- Rouhani, B. D., Garegrat, N., Savell, T., More, A., Han, K.-N., Zhao, R., Hall, M., Klar, J., Chung, E., Yu, Y., Schulte, M., Wittig, R., Bratt, I., Stephens, N., Milanovic, J., Brothers, J., Dubey, P., Cornea, M., Heinecke, A., Rodriguez, A., Langhammer, M., Deng, S., Naumov, M., Micikevicius, P., Siu, M., and Verrilli, C. Ocp microscaling formats (mx) specification. 2023a. URL <https://www.opencompute.org/documents/ocp-microscaling-formats-mx-v1-0-spec-final-pdf>.

- Rouhani, B. D., Zhao, R., More, A., Hall, M., Khodamoradi, A., Deng, S., Choudhary, D., Cornea, M., Dellinger, E., Denolf, K., et al. Microscaling data formats for deep learning. *arXiv preprint arXiv:2310.10537*, 2023b.
- Sakaguchi, K., Bras, R. L., Bhagavatula, C., and Choi, Y. Winogrande: An adversarial winograd schema challenge at scale, 2019.
- See, A., Liu, P. J., and Manning, C. D. Get to the point: Summarization with pointer-generator networks. In *Proceedings of the 55th Annual Meeting of the Association for Computational Linguistics (Volume 1: Long Papers)*, pp. 1073–1083, Vancouver, Canada, July 2017. Association for Computational Linguistics. doi: 10.18653/v1/P17-1099. URL <https://www.aclweb.org/anthology/P17-1099>.
- Shao, W., Chen, M., Zhang, Z., Xu, P., Zhao, L., Li, Z., Zhang, K., Gao, P., Qiao, Y., and Luo, P. Omniquant: Omnidirectionally calibrated quantization for large language models. In *The Twelfth International Conference on Learning Representations*, 2024. URL <https://openreview.net/forum?id=8Wuvvh0LYW>.
- Singh, A., Natarjan, V., Shah, M., Jiang, Y., Chen, X., Batra, D., Parikh, D., and Rohrbach, M. Towards vqa models that can read. In *Proceedings of the IEEE Conference on Computer Vision and Pattern Recognition*, pp. 8317–8326, 2019.
- Sun, X., Choi, J., Chen, C.-Y., Wang, N., Venkataramani, S., Srinivasan, V. V., Cui, X., Zhang, W., and Gopalakrishnan, K. Hybrid 8-bit floating point (hfp8) training and inference for deep neural networks. In Wallach, H., Larochelle, H., Beygelzimer, A., d’Alché-Buc, F., Fox, E., and Garnett, R. (eds.), *Advances in Neural Information Processing Systems*, volume 32. Curran Associates, Inc., 2019. URL https://proceedings.neurips.cc/paper_files/paper/2019/file/65fc9fb4897a89789352e211ca2d398f-Paper.pdf.
- Sun, X., Wang, N., Chen, C.-Y., Ni, J., Agrawal, A., Cui, X., Venkataramani, S., El Maghraoui, K., Srinivasan, V. V., and Gopalakrishnan, K. Ultra-low precision 4-bit training of deep neural networks. In Larochelle, H., Ranzato, M., Hadsell, R., Balcan, M., and Lin, H. (eds.), *Advances in Neural Information Processing Systems*, volume 33, pp. 1796–1807. Curran Associates, Inc., 2020. URL https://proceedings.neurips.cc/paper_files/paper/2020/file/13b919438259814cd5be8cb45877d577-Paper.pdf.
- Talmor, A., Herzig, J., Lourie, N., and Berant, J. Commonsenseqa: A question answering challenge targeting commonsense knowledge, 2019.
- Touvron, H. et al. Llama 2: Open foundation and fine-tuned chat models, 2023.
- Wang, N., Choi, J., Brand, D., Chen, C.-Y., and Gopalakrishnan, K. Training deep neural networks with 8-bit floating point numbers. *Advances in neural information processing systems*, 31, 2018.
- Xiao, G., Lin, J., Seznec, M., Demouth, J., and Han, S. Smoothquant: Accurate and efficient post-training quantization for large language models. *arXiv preprint arXiv:2211.10438*, 2022.
- Yang, J., Kim, H., and Kim, Y. Mitigating quantization errors due to activation spikes in glu-based llms, 2024. URL <https://arxiv.org/abs/2405.14428>.
- Yang, Z., Qi, P., Zhang, S., Bengio, Y., Cohen, W. W., Salakhutdinov, R., and Manning, C. D. Hotpotqa: A dataset for diverse, explainable multi-hop question answering, 2018. URL <https://arxiv.org/abs/1809.09600>.
- Zhang, K., Li, B., Zhang, P., Pu, F., Cahyono, J. A., Hu, K., Liu, S., Zhang, Y., Yang, J., Li, C., and Liu, Z. Lmms-eval: Reality check on the evaluation of large multimodal models, 2024a. URL <https://arxiv.org/abs/2407.12772>.
- Zhang, S., Roller, S., Goyal, N., Artetxe, M., Chen, M., Chen, S., Dewan, C., Diab, M., Li, X., Lin, X. V., Mi-haylov, T., Ott, M., Shleifer, S., Shuster, K., Simig, D., Koura, P. S., Sridhar, A., Wang, T., and Zettlemoyer, L. Opt: Open pre-trained transformer language models, 2022. URL <https://arxiv.org/abs/2205.01068>.
- Zhang, Y., Zhang, S., Cao, S., Du, D., Wei, J., Cao, T., and Xu, N. AFPQ: Asymmetric floating point quantization for LLMs. In Ku, L.-W., Martins, A., and Sriku-mar, V. (eds.), *Findings of the Association for Computational Linguistics ACL 2024*, pp. 28–36, Bangkok, Thailand and virtual meeting, August 2024b. Association for Computational Linguistics. doi: 10.18653/v1/2024.findings-acl.3. URL <https://aclanthology.org/2024.findings-acl.3>.
- Zhao, Y., Lin, C.-Y., Zhu, K., Ye, Z., Chen, L., Zheng, S., Ceze, L., Krishnamurthy, A., Chen, T., and Kasikci, B. Atom: Low-bit quantization for efficient and accurate llm serving. In Gibbons, P., Pekhimenko, G., and Sa, C. D. (eds.), *Proceedings of Machine Learning and Systems*, volume 6, pp. 196–209,

2024. URL https://proceedings.mlsys.org/paper_files/paper/2024/file/5edb57c05c81d04beb716ef1d542fe9e-Paper-Conference.pdf.

Zheng, L., Chiang, W.-L., Sheng, Y., Zhuang, S., Wu, Z., Zhuang, Y., Lin, Z., Li, Z., Li, D., Xing, E., Zhang, H., Gonzalez, J. E., and Stoica, I. Judging LLM-as-a-judge with MT-bench and chatbot arena. In *Thirty-seventh Conference on Neural Information Processing Systems Datasets and Benchmarks Track*, 2023. URL <https://openreview.net/forum?id=ucCHPGDlao>.

A MX FORMAT DETAILS AND EMULATION FRAMEWORK

A.1 MX Configuration

Name	Element Data Type	Element Bits	Group Size	Shared Scale
MXFP8	FP8 (E5M2) FP8 (E4M3)	8	32	8-bit PoT
MXFP6	FP6 (E3M2) FP6 (E2M3)	6		
MXFP4	FP4 (E2M1)	4		
MXINT8	INT8	8		

Table 12. MX-compliant format. Configurations are adapted from (Rouhani et al., 2023a).

As the MX format is our primary focus for improvement, we aim to provide detailed information on it. We follow the MX format configuration and quantization procedure as (Rouhani et al., 2023a;b). The MX format offers a variety of bit-configurations for elements, ranging from 8 bits to 4 bits, while specifying only an 8-bit PoT for the shared scale. The process to determine this 8-bit PoT follows an Algorithm 1. As described in the entire quantization procedure, MX considers the maximum data value to determine the shared scale, performing a floor operation after extracting the exponent of the element’s maximum value with \log_2 .

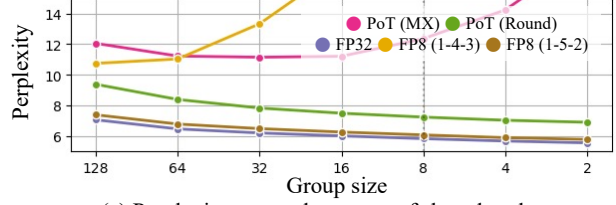
A.2 Determining PoT Shared Scale: Floor vs. Round

As illustrated in Fig. 9(a), an undesirable performance degradation occurs in PoT scales as group size decreases. To analyze this degradation, we decompose the output error into maximum clamping error and rounding error. As shown in Fig. 9(b), with a group size of 2, the rounding error reduces significantly, while the maximum clamping error increases sharply, resulting in a net error rise. This issue is attributed to the floor operation on the exponent in MX, which introduces clamping error. To overcome maximum clamping errors while maintaining the hardware efficiency of PoT shared scales, we replace flooring with rounding. This exponent rounding approach significantly lowers total error, enhancing performance, as demonstrated in Fig. 9(a) and (b).

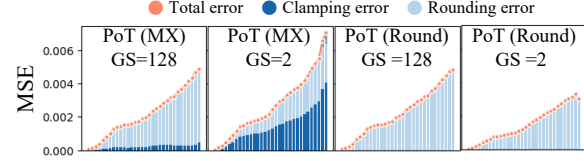
A.3 Code Snippet of Our Framework

As shown in the below example, our proposed AMXFP4 applies different shared scales to positive and negative numbers, enabling more refined value representation compared to MXFP4. Additionally, the PoT shared scale significantly clamps the largest value in the input, 31, to 24, while the FP8 shared scale, using the same number of bits, more precisely quantizes 31 to 30.

```
class MXQuantizer(object):
```



(a) Perplexity across data types of shared scale



(b) Output Error Breakdown

Figure 9. Impact of shared scale (LLaMA2-7B). More results on other models and data formats are in Table 16.

```
def __init__(self, elem_format, group_size,
             scale_mode):
    self.elem_format = elem_format #
        Element Format
    self.group_size = group_size # group
        Size
    self.scale_mode = scale_mode # Shared
        Scale Type
    self.mx_specs = MxSpecs(
        a_elem_format=self.elem_format,
        group_size=self.group_size,
        custom_cuda=True,
        scale_mode=scale_mode,
    )
def quantize(self, x):
    qx = quantize_mx_op(
        x,
        self.mx_specs,
        elem_format=self.elem_format,
        axes=[-1],
    )
    return qx
```

```
# Example: Asymmetrically distributed tensor
with a single row
x = torch.linspace(-4.9, 31, 1024)
```

```
# MXFP4
mx_fp4 = MXQuantizer(elem_format='fp4.e2m1',
                    group_size=-1, scale_mode=0)
qx.mx_fp4 = mx_fp4.quantize(x)
# AMXFP4 (Shared Scale: PoT)
mx_fp4_asym =
    MXQuantizer(elem_format='fp4.e2m1.asym',
                group_size=-1, scale_mode=0)
qx.mx_fp4_asym = mx_fp4_asym.quantize(x)
```


Algorithm 1 Quantization procedure in MX format. Algorithm is adapted from (Rouhani et al., 2023b).

```

1: Quantize vector elements ( $\{V_i\}_{i=1}^k$ ) into MX format
2:  $shared\_exp \leftarrow \lfloor \log_2(\max_i(|V_i|)) \rfloor - max_{elem}$ 
3:  $X \leftarrow 2^{shared\_exp}$ 
4: for  $i = 1$  to  $k$  do
5:    $P_i = \text{quantize}(V_i/X)$ , clamping normal numbers
6: end for
7: return  $X, \{P_i\}_{i=1}^k$ 

```

```

# AMXFP4 (Shared Scale: FP8)
mx_fp4_asym_fp8scale =
    MXQuantizer(elem_format='fp4_e2m1_asym',
                 group_size=-1, scale_mode=152)
qx_mx_fp4_asym_fp8scale =
    mx_fp4_asym_fp8scale.quantize(x)

# Quantized tensor
print(qx_mx_fp4.unique()) # MXFP4
>> tensor([-4., -2., 0., 2., 4., 6., 8.,
           12., 16., 24.], device='cuda:0')
print(qx_mx_fp4_asym.unique()) # AMXFP4 (Shared
    Scale: PoT)
>> tensor([-4.0000, -3.0000, -2.0000, -1.5000,
           -1.0000, -0.5000, 0.0000, 2.0000,
           4.0000, 6.0000, 8.0000, 12.0000,
           16.0000, 24.0000], device='cuda:0')
print(qx_mx_fp4_asym_fp8scale.unique()) #
    AMXFP4 (Shared Scale: FP8)
>> tensor([-5.2500, -3.5000, -2.6250, -1.7500,
           -1.3125, -0.8750, -0.4375, 0.0000,
           2.5000, 5.0000, 7.5000, 10.0000,
           15.0000, 20.0000, 30.0000],
           device='cuda:0')

```

B MORE EXPERIMENTAL RESULTS AND DETAILS

B.1 Experimental Details

Quantization Settings. Our experiments is conducted by modifying the PyTorch and CUDA code within the MX Emulation library (Rouhani et al., 2023b), with exception on Sec. 5.2. We quantize all weights and activations in Transformer decoder layers, including *Query, Key, Self-attention map, and Value*.

Models. The models used in the experiments include OPT (Zhang et al., 2022), LLaMA (Touvron et al., 2023), (AI@Meta, 2024), and Mistral (Jiang et al., 2023), LLaMA2-Chat (Touvron et al., 2023), BART (Lewis et al., 2019), and LLaVA (Liu et al., 2023a) (which backbone is Vicuna-7B (Chiang et al., 2023)).

Language Modeling Tasks. We evaluate on language modeling with WikiText (Merity et al., 2016). The perplexity measurement on the Wikitext test dataset involves grouping 2048 tokens collectively.

Knowledge Evaluation Benchmarks. We evaluate our method into commonsense QA (CSQA) (PIQA (Bisk et al., 2020), WinoGrande (Sakaguchi et al., 2019), ARC challenge (Clark et al., 2018)) and MMLU (Hendrycks et al., 2020). and CSQA and MMLU accuracies are assessed using the lm-evaluation-harness (Gao et al., 2021).

Visual Tasks. For evaluating VLMs, we utilize lmms-eval (Zhang et al., 2024a), including TextVQA (VQA-T) (Singh et al., 2019), DocVQA (Mathew et al., 2021), OCRBench (Liu et al., 2024b), and ChartQA (Masry et al., 2022).

Long-Context Benchmarks. To measure the effectiveness of AMXFP4-FP8 while long-context is given, we utilize LongBench-E (Bai et al., 2024) on LLaMA2-Chat-7B. LongBench-E includes 13 tasks: Qasper (Dasigi et al., 2021), MultiFieldQA (Bai et al., 2024), HotPotQA (Yang et al., 2018), MultihopQA (Ho et al., 2020), GovReport (Huang et al., 2021), MultiNews (Bai et al., 2024), TREC (Li & Roth, 2002), TriviaQA (Joshi et al., 2017), SAMSUM (Gliwa et al., 2019), PassageCount (Bai et al., 2024), PassageRetrieval (Bai et al., 2024), LCC (Guo et al., 2023), and RepoBench-P (Liu et al., 2023b).

B.2 Experimental Details for Sec. 5.2

Quantization Setting in Sec. 5.2. In Sec. 5.2, we compare performance with other studies that apply weight-activation quantization. To determine whether our improved MX format can effectively replace existing techniques for W4A4 inference, we align the experimental settings, applying reduced-precision activations consistent with prior studies. A summary of these results is presented in Table 13. For Table 3, 4, 6, we reproduce the performance of QuaRot and SpinQuant following their official repositories, with modifications to calibration and evaluation datasets. In Table 5, we compare our method against the performance metrics reported for LLaMA by DuQuant (Lin et al., 2024) paper, using models with identical baseline perplexity.

Method	Data Format	Applying Reduced-Precision				
		Attention Operations			Linear Projection	
		Query	Key-Value	Attention Map	Activation	Weight
QuaRot (Ashkboos et al., 2024)	Row-wise Integer	-	✓	-	✓	✓
SpinQuant (Liu et al., 2024c)		-	✓	-	✓	✓
SmoothQuant (Xiao et al., 2022)		✓	✓	-	✓	✓
OmniQuant (Shao et al., 2024)		✓	✓	-	✓	✓
AffineQuant (Ma et al., 2024)		✓	✓	-	✓	✓
QLLM (Liu et al., 2024a)		✓	✓	-	✓	✓
Atom (Zhao et al., 2024)		✓	✓	-	✓	✓
DuQuant (Lin et al., 2024)		✓	✓	-	✓	✓

Table 13. Summary of reduced-precision settings of methods used for comparison in Sec 5.2 experiments.

Robustness Measurement Settings. Following the calibration robustness measurement method introduced in AWQ (Lin et al., 2023), we select two subsets from the Pile dataset (Gao et al., 2020): PubMed Abstracts (of the U.S. National Library of Medicine, 2023) and Enron Emails (Klimt & Yang, 2004). The calibration and evaluation sets are distinct, with no overlap; 128 samples with a sequence length of 2048 are used for calibration, and 200 samples are reserved for perplexity evaluation. Additionally, we configure the calibration set with questions and answers from the PIQA (Bisk et al., 2019) and WinoGrande (Sakaguchi et al., 2019) datasets to analyze calibration effects in question-answering tasks.

B.3 Formula of Integer Quantization

Integer Quantization. The equation for asymmetric integer quantization discussed in Sec. 4.1 is detailed as follows:

$$\hat{x} = \text{Round} \left(\frac{x}{s_x} \right) + z_x, \quad (2)$$

$$z_x = -\text{Round} \left(\frac{x_{\max} + x_{\min}}{2s_x} \right), \quad (3)$$

$$x_q = (\hat{x} - z_x) \cdot s_x. \quad (4)$$

Zero-Point Quantization. When multiplying two asymmetric integers, the operation proceeds as follows:

$$\begin{aligned} x_q \cdot w_q &= (\hat{x} - z_x) \cdot s_x \cdot (\hat{w} - z_w) \cdot s_w \\ &= s_x s_w \cdot (\hat{x} \cdot \hat{w} - z_w \cdot \hat{x} - z_x \cdot \hat{w} + z_x z_w). \end{aligned} \quad (5)$$

where z and s are the zero-point and the integer step size, respectively. When the zero-point of w is treated as zero, an overhead exists in the form of an additional sum $z_w \cdot \hat{x}$ must be added to the partial sum.

B.4 Ablation Study

Ablation Study on Shared-Scale Bit-Encoding. Table 16 illustrates the perplexity according to the type of shared scale across various models and group sizes. In the case of FP4, using the default 8-bit PoT (Floor) shared scale

option of MX, there is a notable increase in perplexity as the group size decreases. This trend is also observed in AsymFP4, primarily due to the increased error from frequent clamping caused by the Floor operation. To address this, our proposed 8-bit PoT consistently improves performance even with smaller group sizes. On the other hand, FP8, another 8-bit alternative, with a 4-bit exponent, significantly degrades performance in models like Mistral, a consequence of its inherent limitations in dynamic range. Conversely, our findings demonstrate that using a 5-bit exponent FP8 shared scale can achieve performance close to FP16.

B.5 Chatbot Results

Fig. 10 presents an example from MT-Bench. While the 16-bit baseline provides responses aligned with the user’s intent, MXFP4 tends to generate repetitive and unhelpful sentences. In contrast, AMXFP4 produces responses that, similar to the baseline, are useful to the user. Table 14 displays the single scores from MT-Bench across different categories. The proposed AMXFP4-FP8 demonstrates the ability to recover baseline performance in most sub-categories.

B.6 LongBench-E Results

Table 15 provides detailed scores for 13 benchmarks in LongBench-E. MXFP4-PoT shows significant performance degradation overall, with a score drop of 16 for contexts exceeding 8K. While MXFP4-FP8 substantially improves over MXFP4-PoT, it still experiences a score reduction of over 6 when handling contexts above 8K. AMXFP4-FP8 increases the average score by more than 2 compared to MXFP4-FP8 for long-context scenarios exceeding 8K.

Question from User: The city of Vega intends to build a bridge that will span the Vegona River, covering a distance of 1.8 kilometers. The proposed location falls within a seismically active area that has experienced several high-magnitude earthquakes. Given these circumstances, what would be the best approach to constructing the bridge?

Response from 16-bit Baseline: Thank you for your question. Building a bridge in a seismically active area requires careful consideration and a multi-faceted approach to ensure the safety of the structure and its users. Here are some key factors to consider:\n1. Seismic Design: The bridge must be designed to withstand earthquakes. This involves using seismic-resistant materials, such as reinforced concrete or steel, and incorporating seismic isolation systems, such as base isolators or seismic isolation bearings. These systems can help reduce the bridge's response to seismic forces, minimizing damage and ensuring continued functionality during earthquakes.\n2. Site Selection: Choose a location for the bridge that is away from potential earthquake fault lines and has a low risk of landslides or other geological hazards. This may involve conducting geological surveys and assessments to identify potential hazards and selecting a site that is safe and stable.\n3. Structural Integrity: The bridge's structural elements, such as the piers, abutments, and superstructure, must be designed to withstand the forces generated by earthquakes. This may involve using reinforced concrete or steel, and incorporating redundancy in the structure to ensure that it can continue to function even if some elements fail during an earthquake.\n4. Foundation Design: The bridge's foundation must be designed to transfer the loads from the bridge to the ground without settling or failing during earthquakes. This may involve using deep foundations, such as piles or caissons, that are capable of resisting lateral loads and settlement. ...

Response from MXFP4-PoT: I'm glad you're interested in building a bridge! Let's explore some considerations first.\n1. Seismic activity: As you've noticed, Vega is an active seismic zone. Given the geological activity, what would be the best approach to constructing the bridge?\n2. Geological constraints: Vega is a volcanic in origin, and the magma is not a problem. The volcanic activity is not a concern for the bridge construction.\n3. Tectonic activity: Vega is a tectonic plate, and the magma is not a problem. The tectonic activity is not a concern for the bridge construction.\n4. Volcanic activity: Vega is a volcanic in origin, and the magma is not a problem. The volcanic activity is not a concern for the bridge construction.\n5. Geological constraints: Vega is a geological hotspot, and the geological activity is not a concern for the bridge construction.\n6. Tectonic activity: Vega is a tectonic spot, and the tectonic activity is not a problem for the bridge construction.\n7. Earthquake activity: Vega is an earthquake-prone area, and the earthquake activity is not a concern for the bridge construction.\n8. Geological constraints: Vega is a geological hotspot, and the geological activity is not a concern for the bridge construction.\n9. Tectonic activity: Vega is a tectonic hotspot, and the tectonic activity is not a concern for the bridge construction.\n10. Geological constraints: Vega is a geological hotspot, and the geological activity is not a concern for the bridge construction.\n1. Volcanic activity: Vega is a volcanic in origin, and the volcanic activity is not a concern for the bridge construction.\n2. Seismic activity: Vega is a seismic in origin, and the seismic activity is not a concern for the bridge construction.\n3. Tectonic activity: Vega is a tectonic hotspot, and the tectonic activity is not a concern for the bridge construction.\n4. Volcanic activity: Vega is a volcanic in origin, and the volcanic activity is not a concern for the bridge construction.\n5. Geological constraints: Vega is a geological hotspot, and the geological activity is not a concern for the bridge construction. ...

Response from AMXFP4-FP8: Thank you for sharing this information. Given the seismic activity in the area, it is crucial to prioritize safety when designing and constructing the bridge. Here are some recommendations for the best approach:\n1. Seismic Design: Incorporate seismic design principles into the bridge's structure and materials. This may include using seismic-resistant materials, such as reinforced concrete or steel, and designing the bridge with seismic loads in mind.\n2. Damping Systems: Implement damping systems to reduce the bridge's response to seismic activity. These can include devices such as shock absorbers or dampers, which can help reduce the bridge's motion and prevent damage from earthquakes.\n3. Reinforced Foundations: Reinforce the bridge's foundations with additional support systems, such as piles or caissons, to ensure stability during seismic activity. This will help prevent the bridge from shifting or collapsing during earthquakes.\n4. Monitoring Systems: Install monitoring systems to track the bridge's condition during seismic activity. This can include sensors to measure movement, strain, or other parameters, which can help identify potential issues before they become major problems.\n5. Emergency Response Plan: Develop an emergency response plan that includes procedures for assessing and repairing damage to the bridge during or after an earthquake. This can help ensure the safety of the bridge and those who use it.\nBy prioritizing safety and incorporating these recommendations into the bridge's design and construction, you can help ensure the safety of the bridge and those who use it during seismic activity. ...

Figure 10. MT-Bench example (LLaMA2-Chat-7B).

AMXFP4: Taming Activation Outliers with Asymmetric Microscaling Floating-Point for 4-bit LLM Inference

Data Format	Writing	Roleplay	Reasoning	Math	Coding	Extraction	STEM	Humanities	Single Score
16-bit Baseline	9.25	7.20	4.65	2.55	3.30	5.55	8.93	9.58	6.38
MXFP4-PoT	4.30	4.05	2.35	1.90	1.25	1.55	5.23	5.15	3.22
MXFP4-FP8	7.20	7.03	3.95	1.70	1.70	4.35	7.53	8.53	<u>5.25</u>
AMXFP4-FP8	8.20	5.98	4.50	2.50	3.05	5.16	7.70	8.70	5.73

Table 14. MT-Bench Single Score (LLaMA2-Chat-7B).

Data Format	Context Length	Single Doc-QA		Multi Doc-QA		Summarization		Few-shot Learning			Synthetic Tasks		Code Completion		Average
		Qasper	MultiField QA	Hotpot QA	Multihop QA	Gov Report	Multi News	TREC	Trivia QA	SAM Sum	Passage Count	Passage Retrieval	LCC	Repo Bench-P	
16-bit Baseline	0-4k	22.99	43.37	37.14	35.79	31.13	26.84	54.00	83.13	39.33	6.35	18.00	62.45	49.02	39.20
	4-8k	18.37	32.29	30.47	24.36	27.89	23.14	60.00	84.02	37.73	2.01	4.00	59.98	48.05	34.79
	8k+	21.42	25.59	24.08	23.37	25.14	23.11	60.00	91.51	40.22	2.72	7.00	56.88	48.51	34.58
MXFP4-PoT	0-4k	12.02	31.91	14.27	15.82	20.23	20.16	32.00	44.39	28.37	4.48	9.42	31.54	34.96	23.04
	4-8k	11.02	17.56	13.83	13.32	15.71	13.96	37.00	36.66	25.93	6.07	2.12	32.13	32.50	19.83
	8k+	9.27	10.26	10.78	10.10	13.94	13.13	36.00	41.83	24.92	5.72	5.09	27.31	35.29	18.74
MXFP4-FP8	0-4k	13.16	40.81	25.27	24.27	22.68	23.66	46.00	77.49	38.97	5.71	9.98	49.54	41.24	32.21
	4-8k	14.26	27.40	21.96	19.36	19.91	18.59	58.00	75.53	35.98	1.50	0.79	48.15	38.45	29.22
	8k+	10.04	23.07	19.15	17.19	18.09	18.66	49.00	79.39	37.82	3.68	5.00	45.10	41.77	28.30
AMXFP4-FP8	0-4k	16.93	34.62	32.16	25.52	23.21	23.49	50.00	76.52	37.88	9.81	10.50	50.76	43.95	33.49
	4-8k	19.56	26.96	26.03	19.74	19.80	19.71	54.00	70.53	36.29	2.04	5.27	48.05	40.77	29.90
	8k+	34.32	17.40	20.52	21.72	18.04	18.70	50.00	79.92	38.73	3.39	9.00	45.12	40.50	30.57

Table 15. Detailed scores of LongBench-E (Bai et al., 2024).

AMXFP4: Taming Activation Outliers with Asymmetric Microscaling Floating-Point for 4-bit LLM Inference

Data Format	Shared Scale	Group Size	OPT		LLaMA2		LLaMA3	Mistral 7B	Qwen
			6.7B	13B	7B	13B	8B	7B	7B
16-bit Baseline			10.860	10.128	5.472	4.884	6.137	5.252	7.605
MXFP4	FP16	128	12.566	12.415	7.065	6.208	9.826	6.137	8.669
		64	11.843	11.958	6.470	5.667	8.368	5.854	8.364
		32	11.475	11.084	6.206	5.444	7.851	5.722	8.214
		16	11.233	10.841	6.015	5.284	7.334	5.607	8.084
	PoT (Floor)	128	24.126	16.151	12.056	11.243	17.848	8.454	10.407
		64	22.605	14.820	11.228	10.453	16.636	8.846	10.023
		32	22.525	14.473	11.150	10.270	16.636	9.454	9.762
		16	23.463	14.638	11.212	10.065	18.582	10.392	9.651
	PoT (Round)	128	40.288	14.460	9.383	8.472	15.741	7.000	9.635
		64	11.878	11.437	6.877	5.898	9.539	6.047	8.671
		32	11.515	10.956	6.432	5.630	8.522	5.855	8.413
		16	11.338	10.689	6.142	5.416	7.628	5.731	8.200
	FP8 (1-4-3)	128	21.914	14.075	10.749	9.883	9.842	55.719	8.783
		64	18.637	15.840	11.036	9.340	8.761	670.647	8.458
		32	24.109	21.447	13.334	9.705	8.733	6050.050	8.358
		16	28.186	33.131	17.082	11.330	8.340	25756.484	8.229
	FP8 (1-5-2)	128	15.857	14.530	7.390	6.450	10.408	6.234	8.806
		64	14.075	12.777	6.788	5.923	8.952	5.957	8.542
		32	13.712	12.091	6.490	5.691	8.307	5.883	8.366
		16	13.534	11.808	6.265	5.520	7.824	5.725	8.247
AMXFP4	FP16	128	12.107	11.718	6.564	5.712	8.364	5.898	8.408
		64	11.489	11.187	6.173	5.400	7.660	5.702	8.272
		32	11.242	10.900	5.999	5.261	7.296	5.588	8.066
		16	11.118	10.581	5.840	5.149	6.978	5.507	7.953
	PoT (Floor)	128	23.161	15.074	11.555	10.839	18.404	8.594	10.123
		64	24.002	14.635	10.956	10.380	18.910	9.217	9.840
		32	25.233	14.569	11.362	10.433	18.748	10.710	9.584
		16	27.992	14.910	12.255	11.118	22.084	14.090	9.595
	PoT (Round)	128	28.781	13.485	8.454	7.466	12.307	6.517	9.235
		64	11.878	11.437	6.877	5.898	9.539	6.047	8.671
		32	11.515	10.956	6.432	5.630	8.522	5.855	8.413
		16	11.338	10.689	6.142	5.416	7.628	5.731	8.200
	FP8 (1-4-3)	128	17.243	13.764	9.725	8.966	8.640	1053.763	8.468
		64	18.093	16.331	10.582	8.622	8.609	3718.406	8.303
		32	20.803	22.674	13.080	9.435	8.193	13421.343	8.231
		16	31.017	40.884	17.459	11.331	8.260	30513.367	8.175
	FP8 (1-5-2)	128	14.580	12.652	6.847	5.901	8.777	6.003	8.568
		64	13.480	12.132	6.451	5.618	8.092	5.817	8.400
		32	13.058	11.902	6.223	5.469	7.725	5.707	8.215
		16	12.941	11.625	6.064	5.374	7.421	5.632	8.114

Table 16. Ablation study on shared scale bit-encoding.

Cluster ID	Centroids		Data Formats						
	Normalized Mean	Normalized Kurtosis	NF4	SF4	INT4	Asym INT4	FP4	Asym FP4	Lloyd-Max
0	0.041	0.003	4.14E-04	5.24E-04	5.77E-04	3.90E-04	5.45E-04	4.65E-04	3.85E-04
1	-0.084	0.472	2.63E-03	1.86E-03	7.06E-03	2.41E-03	2.42E-03	1.43E-03	8.07E-04
2	-0.357	-0.010	4.18E-04	5.70E-04	4.80E-04	3.17E-04	5.40E-04	4.77E-04	3.30E-04
3	0.533	-0.016	3.72E-04	5.27E-04	4.16E-04	2.68E-04	5.44E-04	4.91E-04	2.89E-04
4	0.100	0.577	4.01E-03	2.80E-03	1.06E-02	3.44E-03	3.80E-03	2.19E-03	9.62E-04
5	0.231	-0.002	4.04E-04	5.17E-04	5.55E-04	3.61E-04	5.47E-04	4.71E-04	3.70E-04
6	-0.137	-0.001	4.16E-04	5.39E-04	5.51E-04	3.72E-04	5.41E-04	4.64E-04	3.72E-04
7	-0.236	-0.003	4.20E-04	5.48E-04	5.32E-04	3.52E-04	5.40E-04	4.68E-04	3.59E-04
8	-0.084	0.206	1.13E-03	8.89E-04	2.76E-03	1.18E-03	1.10E-03	7.67E-04	7.36E-04
9	0.353	-0.009	3.83E-04	5.14E-04	4.87E-04	3.18E-04	5.39E-04	4.76E-04	3.33E-04
10	-0.093	0.772	8.39E-03	5.83E-03	2.02E-02	6.59E-03	7.95E-03	4.18E-03	1.60E-03
11	-0.046	0.000	4.10E-04	5.29E-04	5.50E-04	3.78E-04	5.40E-04	4.61E-04	3.73E-04
12	0.096	0.830	1.14E-02	7.93E-03	2.58E-02	8.76E-03	1.09E-02	5.78E-03	1.86E-03
13	0.113	0.279	1.53E-03	1.15E-03	3.93E-03	1.52E-03	1.47E-03	9.78E-04	8.58E-04
14	0.132	0.002	4.12E-04	5.22E-04	5.79E-04	3.84E-04	5.48E-04	4.68E-04	3.86E-04
15	-0.533	-0.016	4.19E-04	5.95E-04	4.12E-04	2.69E-04	5.38E-04	4.85E-04	2.86E-04
Overall Error			1.09E-03	9.74E-04	2.25E-03	9.15E-04	1.17E-03	<u>7.89E-04</u>	4.83E-04

Table 17. Detailed MSE across clusters (LLaMA2-7B Layer 5 QKV-Proj Activations in Wikitext-2 inference).